

Article

The Characteristics of Lithofacies and Depositional Model of Fine-Grained Sedimentary Rocks in the Ordos Basin, China

Zhenhong Chen ¹, Xincheng Li ^{2,*} , Hao Chen ¹, Zhennan Duan ³, Zhen Qiu ¹, Xiaoqian Zhou ² and Yuguang Hou ²

¹ PetroChina Exploration and Development Research Institute, Beijing 100083, China

² Key Laboratory of Tectonics and Petroleum Resources of Ministry of Education, China University of Geosciences, Wuhan 430074, China

³ SINOPEC Gudong Geological Research Institute, Dongying 257000, China

* Correspondence: lxc@cug.edu.cn

Abstract: In order to clarify the characteristics of fine-grained sedimentary lithofacies and the depositional models in lacustrine environments of the Chang 7 Member of the Upper Triassic Yanchang Formation in the Ordos Basin, we focus on the lacustrine lithofacies classification and controlling factors. Based on the typical field sections of the southern Ordos Basin, combined with the methods of organic geochemical analysis, polarizing microscopic observation, XRD and elemental geochemistry, we summarize the main controlling factors of the lithofacies under different sedimentary environments and establish the sedimentary model under different sedimentary backgrounds. Results show that the Chang 7 Member of the Ordos Basin includes six major lithofacies types, i.e., quasi-laminated clayey shale facies, blocky silty mudstone facies, quasi-laminated silty shale facies, laminated silty shale facies, blocky mixed mudstone facies, and laminated argillaceous siltstone facies. Al₂O₃, MgO, CaO, Na₂O, K₂O, and SiO₂ are relatively depleted, while TiO₂, TFe₂O₃, and P₂O₅ are relatively enriched in the Chang 7₂₊₃. Meanwhile, the trace elements are relatively enriched in Cd, Cu, Mo, U, and V. The fine-grained sedimentary facies were influenced by various sedimentary environments, such as paleoclimate, redox conditions, productivity and terrigenous input. According to lithofacies types and genetic mechanisms of the Chang 7 Member in the study area, two types of lithofacies assemblages are identified. The rapid rise in lake level during the deposition of the Chang 7₂₊₃ resulted in an anoxic water column, high productivity, and low terrigenous input under a humid climate and weak-to-moderate weathering conditions. Therefore, clayey shale lithofacies assemblage is developed in the lower Chang 7 Member.

Keywords: lithofacies; sedimentary model; elemental geochemistry; Yanchang Formation; Ordos Basin



Citation: Chen, Z.; Li, X.; Chen, H.; Duan, Z.; Qiu, Z.; Zhou, X.; Hou, Y. The Characteristics of Lithofacies and Depositional Model of Fine-Grained Sedimentary Rocks in the Ordos Basin, China. *Energies* **2023**, *16*, 2390. <https://doi.org/10.3390/en16052390>

Academic Editors: Songtao Wu, Shang Xu, Feng Yang, Juye Shi and Yuanyin Zhang

Received: 1 February 2023

Revised: 23 February 2023

Accepted: 28 February 2023

Published: 2 March 2023



Copyright: © 2023 by the authors. Licensee MDPI, Basel, Switzerland. This article is an open access article distributed under the terms and conditions of the Creative Commons Attribution (CC BY) license (<https://creativecommons.org/licenses/by/4.0/>).

1. Introduction

With the increased exploration and development of conventional oil and gas resources, unconventional hydrocarbon resources have gradually become the focus of hydrocarbon exploration and development over recent years [1]. As an important unconventional oil and gas resource, continental shale oil has attracted sustained attention. The Triassic Chang 7 Member is a typical continental shale oil reservoir in China; previous studies mainly targeted its sedimentary characteristics, reservoir space types and oil-bearing attributes [2]. The Chang 7 oil layer consists mainly of fine-grained deposits characterized by organic-matter-rich shale with thin interbeds of fine sandstone and siltstone. Moreover, the lithofacies heterogeneity presents dominant control over hydrocarbon enrichment [3]. Extensive studies have been carried out on the lithofacies, in particular, the sedimentary environments of marine deposition and marine-continental transition deposition [4–6]. Compared with marine shale, fine-grained sediments in continental lacustrine basins are characterized by a rapid facies transition, abundant mineral components, and complex

stacking configuration [7,8]. Loucks and Ruppel [9] claimed that shale is composed of various lithofacies but predominantly of fine-grained sediments. Furthermore, based on the mineral composition, structure, and fossil and texture identification, three lithofacies were identified, namely laminated siliceous mudstone, calcareous mudstone, and skeletal, argillaceous lime packstone [10]. Over recent years, some studies on continental shale lithofacies have also been reported. Fu et al. [11] divided the Chang 7 deep-water lithofacies into four types. Zhou et al. [12] identified five lithofacies in the Yanchang Formation. A summary of the previous identification schemes of continental shale lithofacies shows that the main criteria include the sediment grain size, structure, bedding, biological feature (fossil), and mineral, and the proposed criteria are highly differentiated [9–12].

Due to the influence of sedimentary environment and evolution, fine-grained sedimentary lithofacies of continental lacustrine basins have strong heterogeneity [13,14]. For example, shale preservation is controlled in dysoxic or anoxic bottom-water environments by limited biological activities and fine-grained sediment consumption [15]. The main control factors of fine-grained sediment enrichment are the paleo-climate, redox conditions of basal water, primary productivity, and terrigenous input, so different sedimentary environments are associated with varied lithofacies assemblages [10,13,15]. Some chemically-stable elements can reflect the properties of parent rocks and record changes in sedimentary paleoenvironments. Moreover, the low porosity and low permeability of fine-grained sediments are favorable for the preservation of such elements. Therefore, the chemical composition of fine-grained sediments enables paleoenvironment restoration [16]. Previous studies suggested that organic-rich fine-grained deposition often occurs under conditions of high productivity, anoxic basal water, and moderate deposition rates, while the fine-grained sediments of the Chang 7 are found with both vertical and horizontal geochemical differentiation [17]. Although extensive work has been done on the paleoenvironment of the Chang 7, it remains controversial or unclear in some aspects, for example, there are prominent differences in the classification criteria and classification scheme of continental fine-grained sediment lithofacies. Redox conditions of the lake basin water column and short-term climate changes during deposition of the Chang 7 are still lacking, which hinders understanding of the development mechanism of continental fine-grained sediments [18,19].

In this research, the deep-water sedimentary outcrop of the Chang 7, which is well exposed in the southern Ordos Basin, is used as an example. Based on the analysis of sedimentary and geochemical characteristics of the profiles, the characteristics of lithofacies under different depositional environments are summarized through organic geochemical analysis, polarizing microscopic observation, and elemental geochemistry. The relationship between lithofacies and multiple environmental factors is established to clarify the development of different lacustrine lithofacies assemblages. It is expected to provide some reference for the exploration and identification of favorable shale oil and gas exploration target intervals, as well as the study of the genesis of deep-water fine-grained sedimentation in the lacustrine basins.

2. Geological Settings

The Ordos Basin is located at the intersection of four different major tectonic regional activities in China. The Qilian-Qinling and Tianshan-Xingmeng fold structure systems lie on the north and south sides of the Ordos Basin, respectively, while the Pacific structural domain and Helan-Liupanshan structural system occur in the east and west. The interior of the basin is divided into six first-order structural units, according to structural morphological characteristics, namely the Yimeng Uplift, Yishan Slope, Weibei Uplift, Jinxi Flexural Fold, Western Margin Thrust Belt, and Tianhuan Depression (Figure 1A) [1]. The combination and superposition of different tectonic domains and various geodynamic environments result in the structural framework in which fault and fold systems mainly develop at the basin margin, and the basin interior is structurally integrated [19]. The main part of the Ordos Basin has always presented itself as a craton basin associated with steady

overall uplifting/subsidence since its formation, which leads to a simple and gentle current geological structure [20]. The crystalline basement of the Ordos Basin was formed during the Archean–Early Proterozoic, and the metamorphic basement ends in the late stage of the Early Proterozoic [21]. During the Early Paleozoic (after the Jinning movement), the basin was subjected to stable uplifting/subsidence, and the typical craton depression was formed within the craton [22,23]. On the basis of the Late Proterozoic–Early Paleozoic crystalline basement and Late Proterozoic–Early Paleozoic marine carbonate platform, the Mesozoic continental basin was finally formed after the Late Paleozoic marine-continental transition deposition. In the Early Mesozoic, the Ordos Basin was influenced by the Indosinian movement. Due to the collision between the North and South China plates, regional uplift occurred in the southern Ordos Basin, forming a large inland lake basin; moreover, due to the late Indosinian movement, the basin was subjected to the overall uplift [19,23]. At the end of the Middle Jurassic, the paleo-Pacific plate movement led to large-scale volcanism, and the regional in situ principal stress direction was Northwest (NW). At this time, the basin began to uplift, which was associated with rapid geothermal temperature elevation, which is considered a vital stage of hydrocarbon generation in the basin. In the Late Cretaceous, compression and uplift of the basin began, which, to a great extent, formed the outline of the present basin [24].

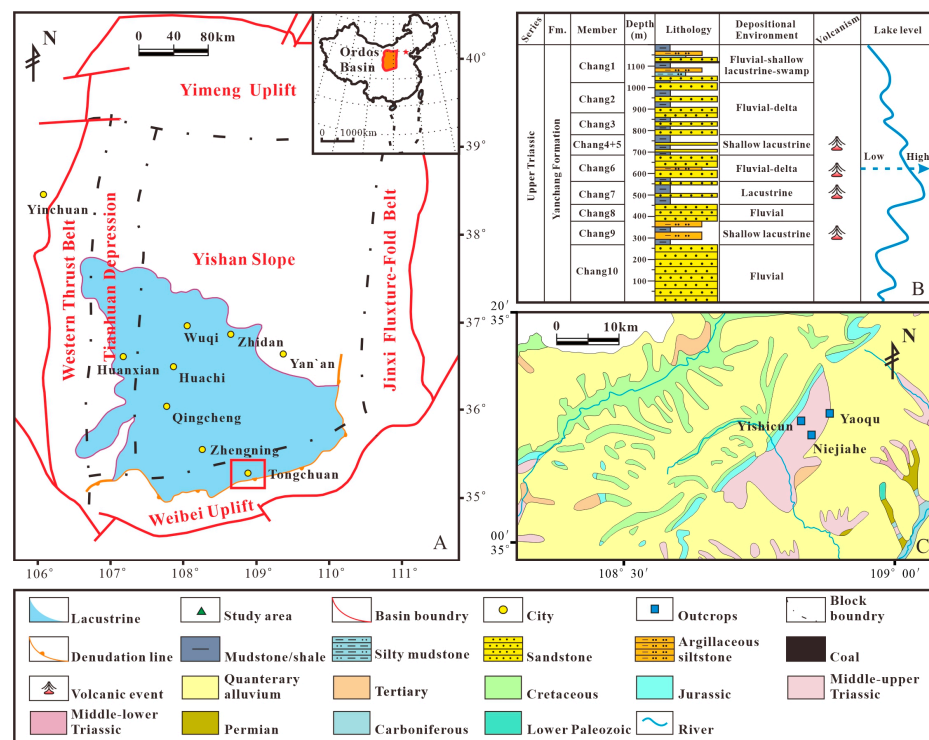


Figure 1. Regional tectonic zone (A), lithology (B) and study area (C) of the Ordos Basin.

During the Indosinian movement, the North China plate, Yangtze plate, and Qinling block collided and merged with each other, and the Qinling-Dabie orogenic belt began to form, which resulted in the common absence of the Upper Triassic in the southern part of North China. The Yanchang Fm. is the strata with the highest surface exposure and the most complete preservation in the northern part of China, and it is also the source rock that first occurred when the basin became the inland lake basin [25]. The average thickness of the Yanchang Fm. is 1300 m, which is divided into 10 oil layer groups (from Chang 10 to Chang 1 Members) from bottom to top (Figure 1B). From the formation stage to the expansion stage of the lake basin, the Yanchang Fm. was mainly of the fluvial or delta facies deposition. During the expansion stage of the lake basin, the central part of the Ordos Basin was dominated by the lacustrine facies, featuring interbedding between

sandstone and mudstone. During the extinction stage of the lake basin, the deposits were mainly composed of fluvial sandstone and mudstone deposits [26]. The Chang 7 was formed during the lake basin expansion stage, during which the lake basin expanded to its largest range, and the lithology was mainly interbedded with black shale, dark mudstone, and sandstone. The lithology of basal Chang 7 Mb. is black shale with siltstone interbeds; that of the middle is mainly dark mudstone; that of the upper part is gray mudstone with siltstone interbeds, argillaceous siltstone, and some siltstone. The lithology of the top of the Chang 7 Mb. transitions to the thick sandstone of the fluvial-facies Chang 6 Mb. [17,24,26].

3. Materials and Methods

3.1. Characteristics of Outcrop Profiles

All samples in this research were collected from the Yaoqu area, Tongchuan City, in the southern margin of the Ordos basin (N 35°10', E 108°51') (Figure 1A). A total of 27 samples were systematically collected from these outcrops. Ten samples were collected from the Ch7₃. Eleven samples were collected from the Ch7₂, and five samples were collected from the Ch7₁ (Figure 2).

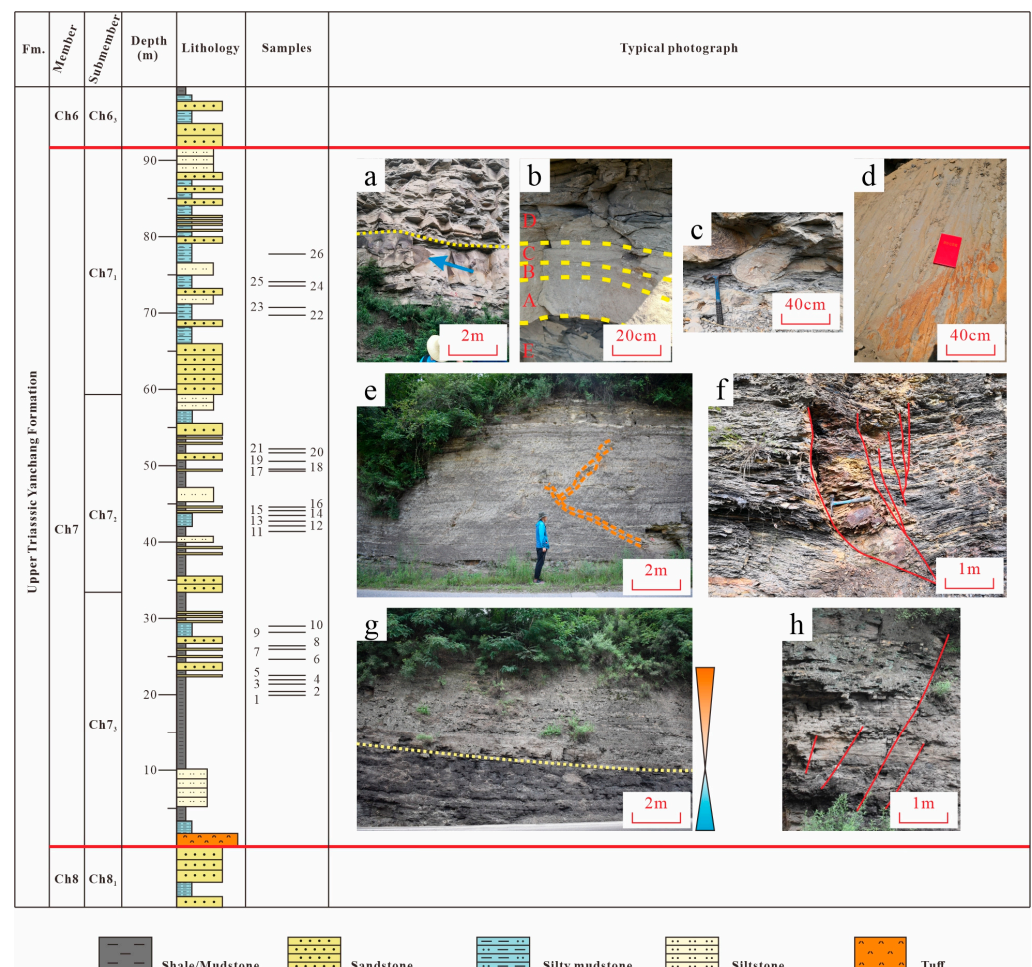


Figure 2. Lithology and typical sedimentary outcrops of the Chang 7 Member in the Ordos Basin. (a) Hydrodynamic transformation of Chang 7₁; the sedimentary section shows that thick sandy clastic rheology changes into thin low-density turbidity sand body, and the blue arrow in the figure indicates rotating structure; (b) Bouma sequence; (c) Load construction; (d) Groove die; (e) The lithology of Chang 7₂ is mainly black shale, and the position circled by orange dotted line in the map is liquefied sandstone vein; (f) Brittle deformation; (g) The bottom of Chang 7₃ is tuffaceous black shale, and the sand content increases upwards, showing that the lake level rises first and then decreases; (h). Stepped fracture.

The Tongchuan area has a typical stratigraphic section of the Chang 7 Mb. of the Upper Triassic Yanchang Fm., which is located at the junction of northwestern Tongchuan County and Zhengning County and includes the Niejiahe Chang 7₃ profile, Yishicun Chang 7₂ profile, and Yaoqu Chang 7₁ profile (Figure 1A,C). It greatly facilitates the systematic investigation of the lithofacies characteristics and genetic models of lacustrine fine-grained sedimentary rocks. The bottom of the Chang 7₃ is in unconformable contact with the underlying deltaic sediments of the Chang 8₁ and presents itself as interbedded between a small amount of medium-thick blocky sandstone and medium-thin shale. The sandstone, the product of sandy debris flows, is mostly developed with a blocky structure. The sediments are upward-fining in the profile. On an overall basis, the Chang 7₃ is thick tuffaceous black shale with thin interbeds of sandstone. It develops macroscopic deformation structures, and stepped faults are observed (Figure 2g,h). The main lithology of the Chang 7₂ is dark shale, with occasionally observed light yellow siltstone interbeds in the middle part and growth of sand content at the top (Figure 2e). The Chang 7₂ is characterized by vertically stacking of black shale with high thickness. The overall rock particle size distribution features the stacking in a fine-coarse-fine manner, which indicates that the Chang 7₂ is of a lacustrine sedimentary system at the junction of the shore-shallow lake and semi-deep lake [27]. Thin tuff occurs inside black shale at relatively high frequencies, which indicates frequent volcanic activity [24]. Local development of medium-thin siltstone is observed, which is attributed to the low-density turbidity current. Macroscopically, localized stepped faults, liquefied crinkled deformation, and sandstone dykes (veins) are seen in the profile of the Chang 7₂, which implies that earthquakes occurred at that time (Figure 2e,f). The Yaoqu profile (the Chang 7₁) is characterized by thick-bedded massive sandstone stacked vertically, with a small amount of gray siltstone interspersed internally, and the thickness of the sand gradually thins upward (Figure 2a). It is shown that the bottom is the typical blocky sand body of the sandy debris flow deposition, featuring structural phenomena such as rotation, deformation, flute cast, groove cast, and boudin structures (Figure 2a–d), which demonstrates that the formations of this profile were formed in an environment with rapid deposition. The extremely thick sand body results from sandy debris flow and represents typical slope gravity flow deposition. The upper part transitions to the sand body of the normal low-density turbidity current, which shows that the Yaoqu area is a lacustrine sedimentary system at the junction of the shore-shallow lake and semi-deep lake and in the proximity of the delta front [2]. In general, the profiles (from the Chang 7₃ to the Chang 7₁) present the reverse grading, showing that the lake level decreases gradually, and thus the sedimentary environment transitions from deep to shallow lake.

3.2. Methodology

3.2.1. Analytical Methods

TOC (Total Organic Carbon) analysis: Samples were ground into powder (>200 mesh) and then treated with the hydrochloric acid (HCl) solution (Volume HCl/water = 1:7) to remove carbonate minerals. Subsequently, TOC content of all samples was measured via combustion with the Elementary Rapid CS Elemental Analyzer Vario EL III.

Mineral composition: About 1–2 g of powder samples was placed and paved on a cover glass, and the XRD analysis was performed using the X' Pert PRO diffractometer. The current was 30 mA; the voltage was 35 kV; the wavelength of the copper target radiation source was $\lambda = 1.54 \text{ \AA}$; the scanning range was $2\theta = 5^\circ\text{--}80^\circ$; the scanning speed was $2^\circ/\text{min}$. The position and amplitude of the diffraction spectrum reflect the crystal structural characteristics, which serve as the basis for identifying each phase and quantifying the corresponding content. The thin section observation was according to the People's Republic of China national standard GB/T 35206-2017. The microstructure of shale was observed using the LEICA DM4500P polarization microscope.

Elemental geochemical analysis: The powder sample (80 μm) was mixed with the lithium borate–lithium nitrate melting flux, and then the even mixture was melted at

1000 °C for 2 h. The melt was poured into a platinum mold to form the flat glass sheet, which was then analyzed using an X-ray fluorescence spectrometer (XRF) to quantify the content of the bulk elements. Two portions of each sample were weighed (approximately 50 mg). One was digested with perchloric acid, nitric acid, and hydrofluoric acid, heated at 190 °C in an oven (>12 h) before being dissolved using the diluted hydrochloric acid to a given volume, and finally analyzed via plasma emission spectrometry (ICP-OES) and plasma mass spectrometry (ICP-MS). The other was evenly mixed with the lithium tetraborate flux, and the mixture was melted in a furnace at above 1025 °C. After the melt was cooled, it was dissolved with nitric acid, hydrochloric acid, and hydrofluoric acid to a given volume and then analyzed using ICP-MS. The results were calibrated using both duplicate analyses of samples and comprehensive analysis. The analytical error was less than 5%.

3.2.2. Data Presentation

Aluminum is resistant to weathering and susceptible to alteration, and thus aluminum concentration is often used as a proxy for clay mineral composition in fine-grained sediments [28]. Al is often used to standardize other trace elements to reduce the effect of detrital content. The enrichment factor (EF) is commonly used to characterize the enrichment degree of each element; this factor reflects the deviation of the concentration of related elements between the tested sample and the mean shale composite and can be calculated as below [29]:

$$EF_{\text{element X}} = (X/Al)_{\text{sample}} / (X/Al)_{\text{PAAS}}, \quad (1)$$

where EF is the enrichment factor of elements. It is normalized using Post Achaean Australian Shale (PAAS) data [30]. $EF > 1$ represents the relative enrichment of the element X in the sample, while $EF < 1$ represents the relative loss of the element X in the sample.

Different elements have different preferences for climate (e.g., humid and arid environments) [31]. For example, Fe, Mn, Cr, Ni, V, and Co tend to enrich in humid environments, while Ca, Mg, Sr, Ba, K, and Na tend to accumulate in dry environments. Therefore, the ratio (C value) of the above two types of elements can reflect the paleoclimate of the study area. The larger the C value is, the wetter the climate conditions are during deposition [32]. The C-value is calculated using the following formula:

$$C\text{-value} = \Sigma (\text{Fe} + \text{Mn} + \text{Cr} + \text{Ni} + \text{V} + \text{Co}) / \Sigma (\text{Ca} + \text{Mg} + \text{Sr} + \text{Ba} + \text{K} + \text{Na}), \quad (2)$$

The chemical index of alteration (CIA) is often used as a measure of weathering intensity [33] and is calculated using the following formula:

$$CIA = 100 \times Al_2O_3 / (Al_2O_3 + CaO^* + Na_2O + K_2O), \quad (3)$$

CaO* represents CaO in silicate (in other words, the bulk rock CaO minus the mole fraction of chemically deposited CaO) and is calculated as $CaO^* = CaO - (10/3 \times P_2O_5)$, and the smaller value between Na₂O and CaO is taken as the mole number of CaO* after correction [33]. CIA values can be divided into 50–65, 65–85, and 85–100 to characterize the alteration intensity from weak to strong.

4. Results

4.1. Characteristics of Organic Matter

TOC is an important measure of hydrocarbon generation. Based on the TOC analysis of the Upper Triassic Chang 7 Mb. shale samples in the study area, this research investigated the vertical variation of organic matter abundance in the Chang 7 Mb. shale. The TOC measurements show that the Chang 7 Mb. shale is generally seen with enrichment of organic matter, and the TOC ranges from 0.72% to 24.86%, with an average of 9.16%, indicating that the organic matter content of the Chang 7 Mb. shale is highly heterogeneous. In view of the vertical distribution, the TOC is high in the lower part (1.51–24.86% in

the Chang 7₂₊₃, with an average of 13.34%) and low in the upper part (0.80–1.85% in the Chang 7₁, averaging 1.02%). The TOC of the Chang 7₂ is relatively moderate (1.52–18.38%, averaging 8.99%). The TOC of the Chang 7₁ profile is generally <2.0%, and with the increase of burial depths, it is generally >2.0% in the Chang 7₂ profile; the Chang 7₃ profile is >2.0% (mostly >6.0%).

The polarization microscope reveals considerable differentiation in occurrence states of organic matter. Three states of organic matter are observed and identified under the microscope (Figure 3): (1) The organic matter presents itself as banded or laminated parallel bedding, and the common occurrence is interbedding between organic matter and clay minerals or between organic matter, silt, and clay minerals (Figure 3A,B). (2) The organic matter is seen with dotted or flocculent distribution, with occasionally observed rock debris (Figure 3C,D). (3) The organic matter is distributed in an irregular patchy style with discontinuous laminations (Figure 3E,F).

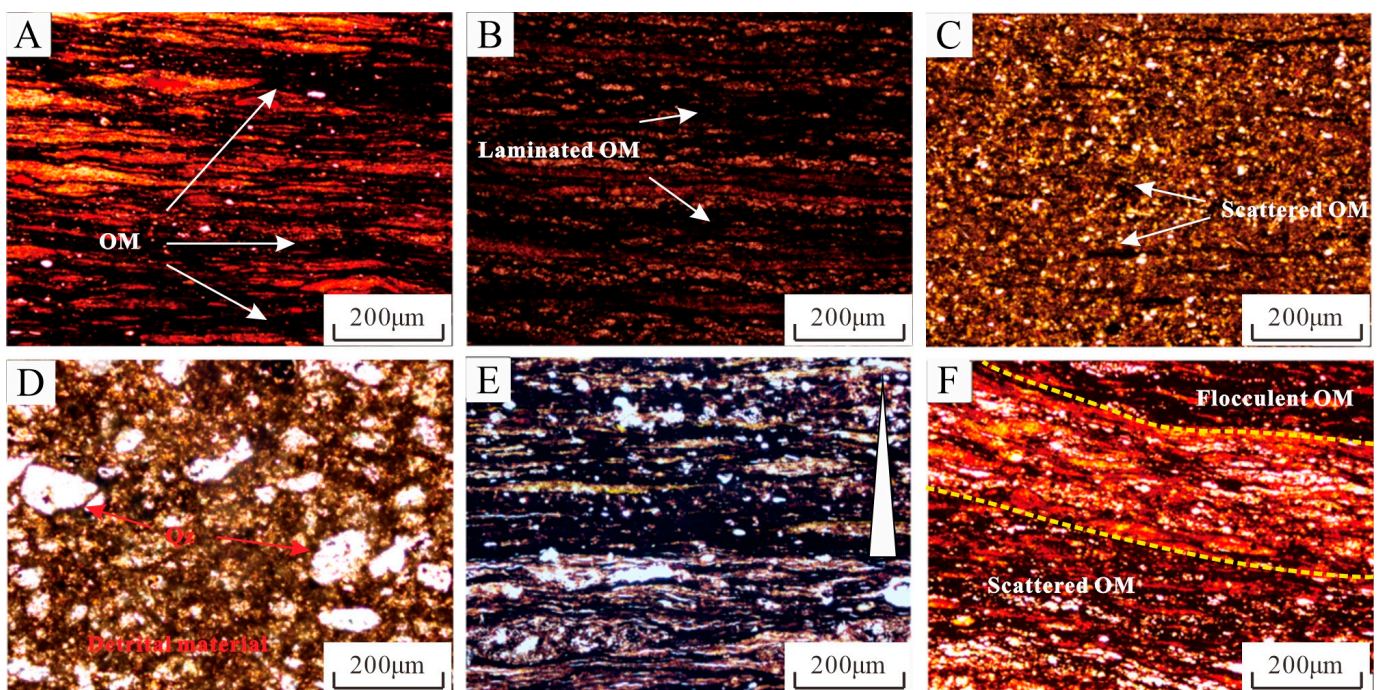


Figure 3. Organic matter distribution in the Chang 7 shales of the Ordos Basin. (A) Laminated organic matter, Sample 2; (B) laminated organic matter with dotted silt, Sample 4; (C): patchy organic matter, Sample 21; (D) calcite seen within organic matter bands, Sample 24; (E) the scattered organic matter with high silty sand content, Sample 10; (F) uneven distribution of organic matter, Sample 7. OM = Organic matter; Qz = Quartz.

4.2. Lithofacies Classification

At present, scholars apply highly different methods to lithofacies classification of continental shale, such as those based on macroscopic sedimentary characteristics (structures, textures, etc.), mineral composition, TOC, and fossil assemblages [11,12]. On the basis of the outcrop description, the shale lithofacies of the Chang 7 Mb. are grouped in terms of the mineral composition, TOC, structure, texture, and lamination morphology of mudstone/shale. At present, the three-unit diagram of felsic-clay-carbonate minerals is widely used to divide lithofacies, and Diaz et al. [34] made a more detailed division of shale lithofacies. A scheme of four lithofacies assemblages for the mudstone/shale is proposed for the study area, in view of the ternary diagram based on the carbonate mineral content, clay mineral content, and siliceous mineral content. Specifically, the four assemblages are siltstone, limestone, clayey shale, and mixed shale facies (Figure 4). Moreover, the above

four lithofacies assemblages can be sub-divided into 10 lithofacies in accordance with the content thresholds of 25%, 50%, and 75% of the three end-member minerals.

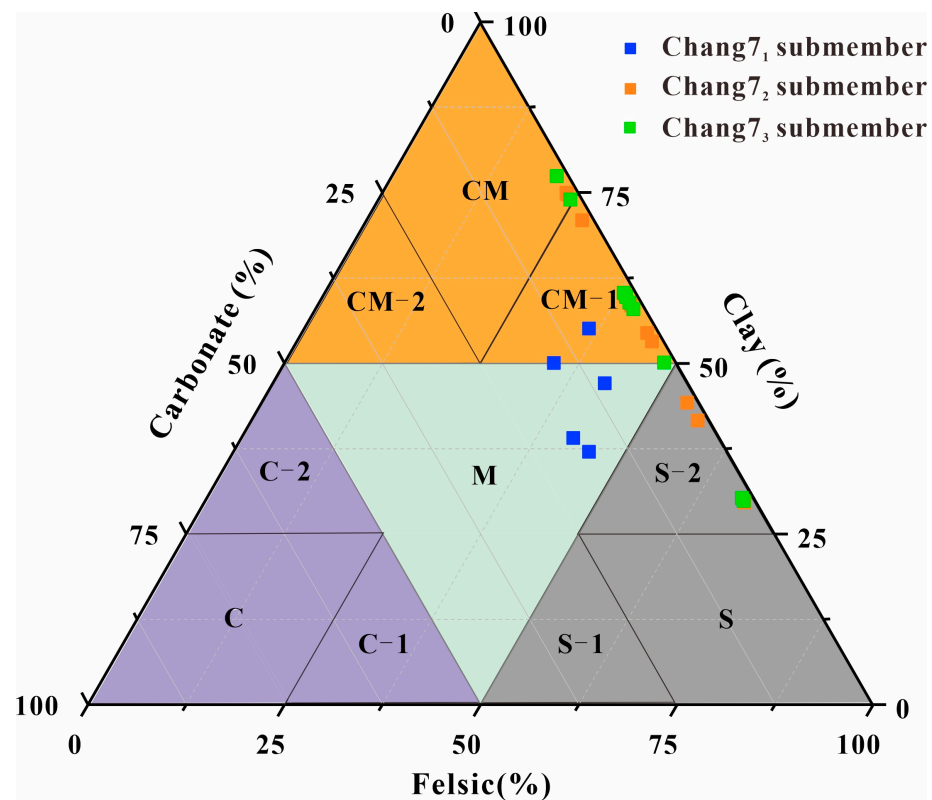


Figure 4. Three-terminal element diagram of shale mineral composition. For the siltstone lithofacies assemblage, S: siltstone facies, S-1: calcareous siltstone facies, and S-2: argillaceous siltstone facies; for the limestone lithofacies assemblage, C: limestone facies, C-1: silty limestone facies, and C-2: argillaceous limestone facies; for the shale lithofacies assemblage, CM: clayey shale facies, CM-1: silty shale facies, and CM-2: calcareous shale facies; for the mixed lithofacies assemblage, M: mixed facies.

4.2.1. Quasi-Laminated Clayey Shale Facies (CM)

The quasi-laminated clayey shale facies are mainly distributed at the bottom of the Chang 7₃, with dozens of thin tuffaceous strips visible in outcrops (Figure 2g). Under the microscope, organic matter is seen with intermittent distribution accompanied by inclusions of detrital minerals, framboidal pyrite, collophanite, and fossils (Figure 5A,B). The quasi-laminated clayey shale has been formed under the influence of volcanic activities and has an extremely high TOC (averaging 16.16%). The color of this lithofacies is mainly black and black-gray. The clayey shale facies are formed in a deep-water environment associated with volcanic eruptions. It presents a quasi-laminated structure and extremely high content of clay minerals (>75%).

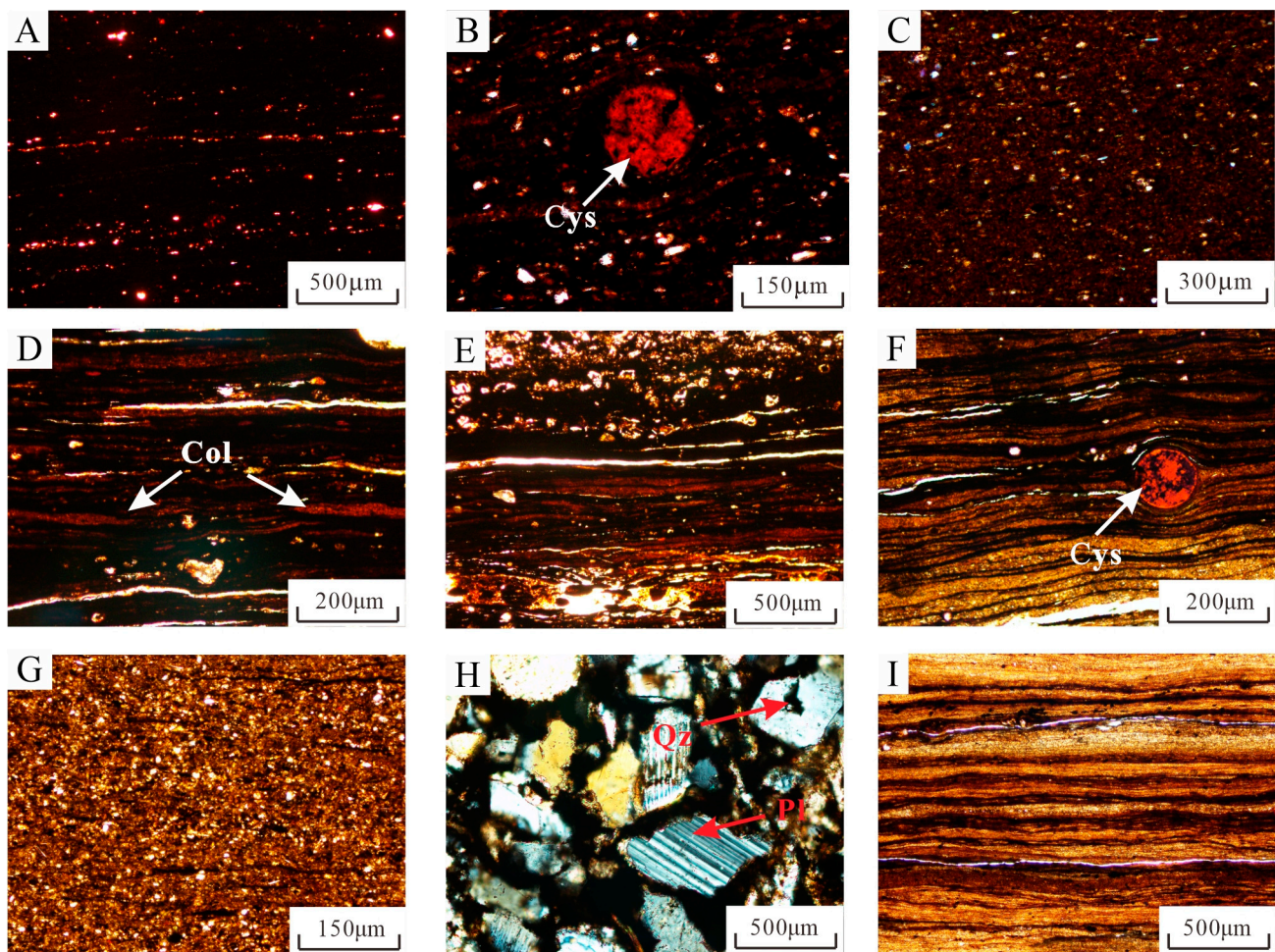


Figure 5. Microscopic characteristics of fine-grained sedimentary lithofacies in the Chang 7 member, Ordos Basin. (A) Quasi-laminated clayey shale facies with the intermittent distribution of organic matter and observed bright detrital minerals, Sample 1; (B) quasi-laminated clayey shale facies with metasomatic replacement of algal fossils by red collophanite, Sample 1; (C) blocky silty mudstone facies with underdeveloped laminations, Sample 11; (D,E) quasi-laminated silty shale facies with discontinuous organic matter and numerous inclusions of collophanite, Sample 8; (F) laminated silty shale facies with highly developed laminations and algal fossils, Sample 9; (G) blocky mixed mudstone facies with the dotted distribution of organic matter and many detrital particles, Sample 21; (H) blocky mixed mudstone facies (under the cross-polarized light) with observed quartz and feldspar particles, Sample 21; (I) laminated argillaceous siltstone facies with alternating sandy and clayey laminations, Sample 18. Cys = Cystocarp fossil; Col = Collophanite; Qz = Quartz; Pl = Plagioclase.

4.2.2. Blocky Silty Mudstone Facies (CM-1)

The blocky silty mudstone mainly occurs in the middle of the Chang 7₂. The lithofacies are gray-black, with a blocky texture and underdeveloped laminations (Figure 5C). It is formed at the junction of the deep water and shallow water of the slope break zone. Compared with the clayey shale facies, these facies have a considerably higher content of siliceous minerals, and the organic matter is distributed in a dotted flocculent manner. Under the plane-polarized light microscope, a large number of quartz, feldspar, and calcite mineral particles are observed with the dotted distribution. These particles, which are rectangular and triangular, are less rounded. The deposition of this facies may be subjected to bioturbation at the oxidation interface and organic matter degradation, which results in low organic matter content [29].

4.2.3. Quasi-Laminated Silty Shale Facies (CM-1)

The quasi-laminated silty shale facies are mainly distributed in the lower part of the Chang 7₂, which is gray-brown and formed in the deep-water environment of the semi deep-lake facies. This lithofacies consists of 36% felsic and 64% clay, and the overall siliceous mineral content is low. Feldspar and quartz particles are occasionally seen under the microscope; the average TOC content is 9.19%. Collophanite is abundant, and fossils can be observed, which shows that it is less affected by the continental margin (Figure 5D,E). Organic matter and clay minerals are suspended and settled together via complexation, and the interface between organic matter and clay minerals is ambiguous, which is the main feature that distinguishes this lithofacies from another high-TOC laminated lithofacies.

4.2.4. Laminated Silty Shale Facies (CM-1)

The laminated silty shale is mainly distributed in the middle of the Chang 7₃ Sub-Member and the middle of the Chang 7₂. The lithofacies appear to be black, and tuffaceous bands can be seen in outcrops (Figure 2e–g). It is deposited in a deep-water environment, with well-developed laminations. It contains 45% felsic and 55% clay, and TOC is 8.41%. The thin section petrographic analysis shows that clay, organic matter, and sandy laminations are generally associated with the wavy and linear continuous distribution and dashed discontinuous distribution. Microscopically, spherical or near-spherical algal fossils with collophanite shells and bright laminations formed by framboid pyrite can be seen, which reflects that the sedimentary environment at that time was anoxic and had extremely high productivity (Figure 5F).

4.2.5. Blocky Mixed Mudstone Facies (M)

The blocky mixed mudstone is mainly distributed at the bottom of the Chang 7₁, and the lithofacies is gray. The thin section petrographic analysis shows that the lithofacies presents suppressed development of laminations. The sedimentary environment is shallow water of the shore-shallow lake-delta front facies. It is composed of 41% felsic, 43% clay, and 16% carbonate minerals, and the carbonate mineral content is relatively high. Under the plane-polarized light, a large number of mineral particles, such as quartz, feldspar, and calcite, can be seen, which are rectangular and triangular, and the textural maturity is low (Figure 5G,H). On an overall basis, this facies features sufficient terrigenous input, proximity to the estuary provenance, and high sandy content during the deposition. Due to high terrigenous input, the TOC content is 0.72–1.85%, with an average of 1.07%, which leads to intermittent occurrence of organic matter veins and low organic carbon content in mudstone.

4.2.6. Laminated Argillaceous Siltstone Facies (S-2)

The laminated argillaceous siltstone is one of the main lithologic components of the Chang 7 Mb. and mainly occurs in the middle of the Chang 7₂. The outcrop is gray-black and shows that the lower part of this interval in the study area is interbedded between thin shale and argillaceous siltstone, and the upper part is interbedded with thin siltstone and mudstone (Figure 2E). The sedimentary environment is shallow lake–semi-deep lake facies, and the mineral composition is 55–70% siliceous (averaging 62%) and 38% clay. Laminations are well developed, and the boundary between sandy and organic laminations is clear under the microscope (Figure 5I). The formation of sandy bands is mostly affected by paroxysmal events like turbidity currents, and the supply of terrigenous detrital materials is sufficient [2].

4.3. Elemental Geochemical Characteristics

4.3.1. Bulk Oxide

The main oxide components in the study area are SiO₂, Fe₂O₃, and Al₂O₃ (>5%) (Table 1). It can be seen from the EF distribution of the main elements of the Chang 7 shale (Figure 6A) that compared with the corresponding PAAS, the variation trends of main

elements in the Chang 7₃ and Chang 7₂ are similar. The EFs of Al₂O₃, TiO₂, K₂O, Na₂O, and SiO₂ are like those of PAAS. MgO shows deficits relative to the PAAS (EFs < 1), while CaO, TFe₂O₃, and P₂O₅ are enriched (EFs > 1). The content of SiO₂ is 32.89–64.05% (average is 48.94%), which shows that the content of quartz is high in rocks. Al₂O₃, Na₂O, and K₂O mainly occur in clay minerals, and their content is close to the PAAS mean values, which indicates that clay minerals may come from the continental crust; the average enrichment factor of MgO is 0.62, which is far lower than the PAAS mean value. Feldspar and dolomite are relatively active minerals (prone to alteration); thus, Mg is usually removed from rocks by invaded solutions during chemical weathering, resulting in the decrease of its enrichment factors [30]. Ca has many occurrence forms and is commonly founded in calcite and clay minerals. As indicated by the microscopic characteristics, the detrital mineral content during the deposition of the Chang 7₁ is high, and correspondingly, Ca is strongly enriched; for Ti, this is indicative of the stability of terrigenous detrital supply, the content of TiO₂ is similar to the PAAS mean content (EF = 0.8), which indicates that terrigenous detrital supply is stable during deposition of the Chang 7 Mb. [35]; for Fe, this is often related to pyrite and commonly used to represent the redox condition, the content of TFe₂O₃ is relatively high and indicates that the overall lake basin is in a reductive state at that time [36]; in addition, P₂O₅ is enriched in the Chang 7₃ and Chang 7₂ and yet deficient in the Chang 7₁, with an average EF of 1.17, which demonstrates the high content of organic matter and primary productivity of the Chang 7 shale [37].

Table 1. Major element contents (wt.%) of the Chang 7 Member.

Mb.	No.	SiO ₂	TiO ₂	Al ₂ O ₃	TFe ₂ O ₃	MgO	CaO	Na ₂ O	K ₂ O	P ₂ O ₅
Chang 7 ₁	S. 1	52.12	0.65	15.62	4.96	2.37	7.66	0.73	3.00	0.14
	S. 2	51.16	0.65	15.73	5.48	2.45	8.30	0.70	3.01	0.14
	S. 3	51.81	0.60	13.46	4.69	2.38	10.15	0.80	2.55	0.13
	S. 4	51.73	0.61	13.74	4.73	2.40	9.99	0.82	2.62	0.13
	S. 5	53.78	0.76	18.40	5.44	2.93	4.36	0.74	3.61	0.14
Chang 7 ₂	S. 6	42.71	0.44	13.09	7.88	0.71	0.67	0.73	2.74	0.40
	S. 7	50.72	0.54	14.66	9.05	0.84	1.18	0.84	3.02	0.36
	S. 8	44.15	0.48	11.48	9.72	0.71	1.72	0.96	2.16	0.57
	S. 9	35.23	0.39	9.44	9.38	0.69	1.66	0.63	2.04	0.27
	S. 10	62.39	0.45	10.69	7.42	0.57	0.71	0.80	2.20	0.28
	S. 11	44.47	0.37	10.23	7.62	0.47	1.80	1.09	1.89	0.38
	S. 12	50.84	0.52	14.61	9.72	0.56	0.72	0.82	3.95	0.39
	S. 13	47.32	0.55	13.11	6.34	0.69	0.97	0.66	3.48	0.26
	S. 14	59.74	0.49	16.93	6.69	0.09	0.42	0.40	4.19	0.43
	S. 15	64.05	0.51	13.60	4.21	0.57	0.57	0.80	3.36	0.17
Chang 7 ₃	S. 16	39.56	0.46	11.65	8.29	0.82	1.75	0.86	2.50	0.28
	S. 17	37.20	0.43	12.36	8.59	0.67	1.32	0.88	2.12	0.55
	S. 18	32.89	0.42	8.79	6.96	0.39	1.52	0.59	1.98	0.20
	S. 19	49.34	0.45	13.63	6.23	0.52	0.56	0.77	2.86	0.27
	S. 20	39.18	0.41	9.52	2.92	0.42	1.43	0.78	1.80	0.19
	S. 21	51.39	0.42	11.78	5.81	0.58	0.56	0.89	2.81	0.18
	S. 22	44.15	0.45	6.75	5.30	0.63	1.74	0.42	1.38	0.13
	S. 23	45.55	0.55	10.42	9.94	0.46	1.46	0.70	2.01	0.28
	S. 24	44.90	0.50	10.82	7.91	1.20	2.06	0.84	2.06	0.11
	S. 25	54.69	0.63	17.12	8.01	1.32	0.83	0.89	3.68	0.15
	S. 26	62.16	0.68	19.79	2.68	1.05	0.68	0.93	3.81	0.07

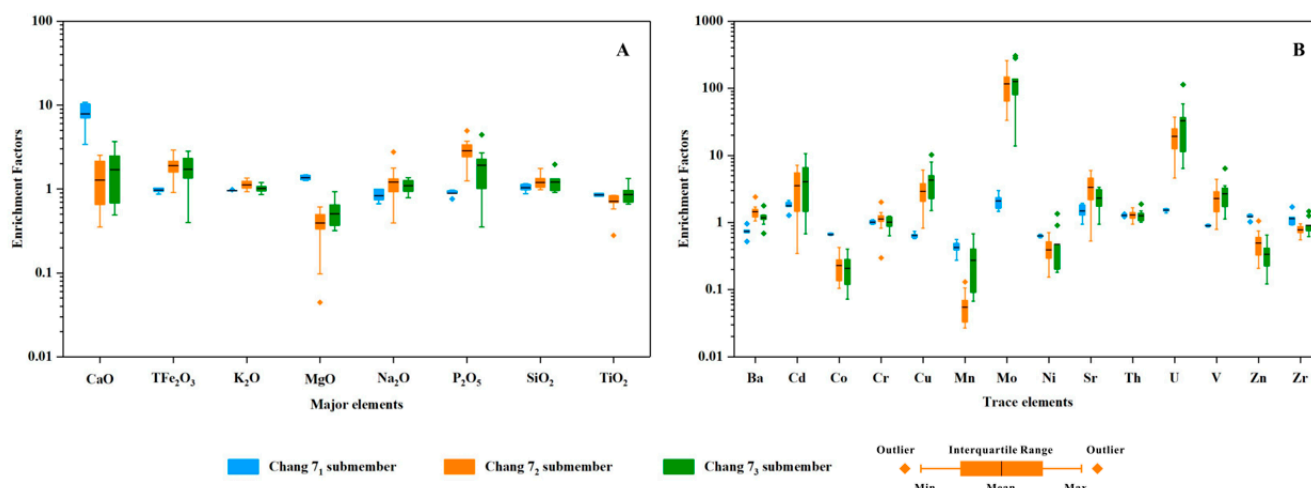


Figure 6. (A) Enrichment factors of the selected major elements relative to the PAAS [25] for the Chang 7 Member.; (B) EFs of trace elements of the Chang 7 Member.

4.3.2. Trace Elements

The variation of trace elements in the Chang 7 fine-grained sediments can be used to restore the paleoenvironment during deposition, including the paleoclimate, paleo-productivity, paleo-redox conditions, and paleodepth. Influenced by the sedimentary environment, different lithofacies of the Chang 7 Mb. are highly differentiated in their planar and vertical distribution [38]. The analysis results for trace elements (Figure 6B, Table 2) show that the states of trace elements can be divided into three types: (1) the enrichment type ($EF > 1$), for example, the elements Cd, Cu, Mo, U, Sr, and V are relatively enriched; (2) the similar type, with the enrichment factor close to 1, e.g., Ba, Cr, and Th; and (3) the loss type ($EF < 1$), including Co, Ni, Zn, and Zr. According to the above classification, it can be seen that the Chang 7₂₊₃ are rich mainly in sensitive elements, which greatly change with paleo-redox conditions. The change of the sedimentary environment during the deposition of the Chang 7 Mb. is the main reason for the enrichment or loss of different trace elements, which leads to the enrichment differentiation of elements among the different fine-grained sediments.

In fine-grained sediments with abundant organic matter, the enrichment factor of Cu, a bio-element, usually reflects the high primary productivity of sedimentary water columns [17]. Mo, V, and U are sensitive to redox conditions, and their content is greatly affected by different redox conditions, depending on their different chemical properties. Therefore, the enrichment and loss of these elements in sediments are indicative of the redox conditions of water columns [39,40]. Usually, the element U in an oxidizing water column presents itself in the +6 valence state, and it is easy to form stable $UO_2(CO_3)_4^{3-}$; on the contrary, it usually precipitates in the form of the hydroxyl complex under reductive conditions [38]. V and Mo also have the ability to change valence and tend to be enriched under reductive conditions [38–41]. Ba and Sr are greatly affected by the salinity of the sedimentary environment, and Sr/Ba is often used as an index of paleo-salinity [42]. The loss of these two elements indicates that the salinity of water columns was not high during the lake basin deposition of the Chang 7 Mb. [42]. Thorium has the lowest response to redox conditions. It is seldom dissolved and tends to adhere to sediments [39]. Cr often participates in the composition of detrital minerals in fine-grained sediments and can adhere to clay by replacing Al [39]. Its chemical composition is relatively stable under reductive conditions [16]. Ni, Zn, and Co are affected by climate and are prone to weathering reactions, which results in the relative loss of these elements in sediments [43].

Table 2. Trace element contents (ppm) of the Chang 7 Member.

Mb.	No.	Ba	Cd	Co	Cr	Cu	Mn	Mo	Ni	Sr	Th	U	V	Zn	Zr
Chang 7 ₁	S. 1	527.00	0.16	12.70	100.00	27.90	382.00	1.81	31.30	219.00	15.60	4.30	112.00	92.00	165.00
	S. 2	394.00	0.14	12.80	90.00	28.10	370.00	2.10	29.00	248.00	15.25	3.70	116.00	94.00	167.00
	S. 3	374.00	0.15	11.80	90.00	21.70	403.00	2.34	26.40	290.00	14.45	3.70	96.00	85.00	268.00
	S. 4	375.00	0.13	11.40	80.00	23.20	474.00	1.31	26.80	283.00	14.45	3.70	106.00	79.00	195.00
	S. 5	334.00	0.12	15.80	110.00	36.20	298.00	1.50	32.20	185.50	18.45	4.60	140.00	86.00	195.00
Chang 7 ₂	S. 6	633.00	0.11	1.70	90.00	109.50	21.00	108.50	11.00	474.00	14.45	46.70	263.00	18.00	110.00
	S. 7	673.00	0.34	4.80	90.00	106.50	92.00	70.50	15.30	468.00	13.50	42.30	244.00	43.00	113.00
	S. 8	650.00	0.29	3.60	70.00	85.60	27.00	92.70	16.40	651.00	11.65	52.70	253.00	23.00	109.00
	S. 9	553.00	0.28	2.40	110.00	89.40	19.00	134.50	17.00	425.00	10.75	43.70	330.00	15.00	95.00
	S. 10	401.00	0.12	4.20	90.00	68.90	58.00	42.00	11.00	429.00	11.25	22.80	187.00	28.00	105.00
	S. 11	530.00	0.37	3.10	50.00	115.50	22.00	73.20	21.40	658.00	8.66	34.60	247.00	23.00	110.00
	S. 12	749.00	0.23	4.40	90.00	80.40	39.00	72.60	13.20	478.00	10.80	29.40	178.00	25.00	100.00
	S. 13	509.00	0.44	4.70	90.00	139.50	22.00	100.00	20.60	176.00	13.35	48.10	290.00	28.00	130.00
	S. 14	779.00	0.03	9.00	30.00	48.30	132.00	31.60	15.60	97.30	15.40	44.20	109.00	82.00	107.00
	S. 15	501.00	0.09	2.10	90.00	75.50	33.00	44.90	8.10	204.00	13.20	28.50	150.00	13.00	112.00
Chang 7 ₃	S. 16	576.00	0.23	2.10	80.00	192.00	33.00	139.00	13.00	466.00	13.00	73.00	306.00	15.00	109.00
	S. 17	496.00	0.30	6.40	70.00	78.00	168.00	97.80	16.00	184.00	10.15	24.40	232.00	38.00	89.00
	S. 18	385.00	0.29	3.60	50.00	116.00	93.00	148.00	11.80	196.50	7.85	46.50	245.00	19.00	87.00
	S. 19	547.00	0.13	2.30	70.00	130.50	116.00	69.20	7.30	465.00	14.55	48.80	283.00	16.00	116.00
	S. 20	377.00	0.26	2.70	70.00	260.00	111.00	149.00	10.80	179.50	8.53	92.80	487.00	16.00	88.00
	S. 21	519.00	0.10	1.70	60.00	91.00	62.00	51.70	10.10	332.00	11.80	70.60	181.00	16.00	117.00
	S. 22	269.00	0.23	2.40	50.00	147.50	273.00	45.10	18.40	209.00	10.15	131.00	181.00	12.00	97.00
	S. 23	666.00	0.08	1.30	40.00	61.80	257.00	70.50	12.30	385.00	8.95	46.90	150.00	6.00	177.00
	S. 24	463.00	0.60	3.50	80.00	139.00	449.00	54.60	44.60	372.00	12.95	26.80	230.00	21.00	114.00
	S. 25	579.00	0.07	3.00	110.00	129.00	93.00	36.00	10.40	365.00	15.15	25.20	227.00	18.00	155.00
S. 26	484.00	0.07	1.80	120.00	81.60	81.00	15.60	10.90	204.00	16.15	21.70	183.00	16.00	160.00	

5. Discussion

5.1. Main Control Factors of Fine-Grained Sediment Lithofacies

The change of lithofacies is often influenced by periodic sedimentary changes and unexpected events during deposition [13]. The paleo-environment of fine-grained sediments, including the paleoclimate, redox conditions, paleo-productivity, and terrigenous input, is analyzed in view of the results of bulk and trace elements in the study area.

5.1.1. Paleoclimate

The paleoclimate affects the lake environment and organic matter enrichment by dominating exogenous and endogenous deposition in the basin [44]. Therefore, the relative concentrations of particular elements can be used to reconstruct paleoclimate environment [45,46]. C-values >0.8 reflect a humid paleoclimate, values from 0.2 to 0.8 are correlated to a semiarid–semihumid paleoclimate, and values <0.2 suggest an arid paleoclimate [32]. The C value of the Chang 7 Mb. is in the range of 0.29–1.69, with an average of 1.02 (greater than 0.8), indicating that the overall deposition of the Chang 7 Mb. proceeded in a humid environment (Figure 7A). However, different lithofacies have different C values. The mixed mudstone facies (M) are deposited in the semi-arid climate; the clayey shale facies (CM) are deposited in a humid environment; the other lithofacies can occur in different climates. The Sr/Cu ratio can also be used to represent paleoclimate. For this ratio, Cu is considered wetting-preferring and therefore, similar to the C value, larger Sr/Cu represents the drier paleoclimate of the lake basin. Clearly, in C value versus Sr/Cu, the main distribution range of Sr/Cu of the samples is 0.69–7.61, with an average of 3.64, except for the mixed mudstone facies (M) (with an average of 10.56). This also shows that the Chang 7 Mb. was developed in a relatively humid environment. High CIA reflects strong chemical alteration and, furthermore, a relatively warm and humid environment with high weathering degrees, which is unfavorable for the preservation of organic matter. The calculated CIA of the samples from the Chang 7 Mb. is 64.49–77.46, with an average of 71.03, showing moderate weathering and warm and humid paleoclimate conditions (Figure 7B).

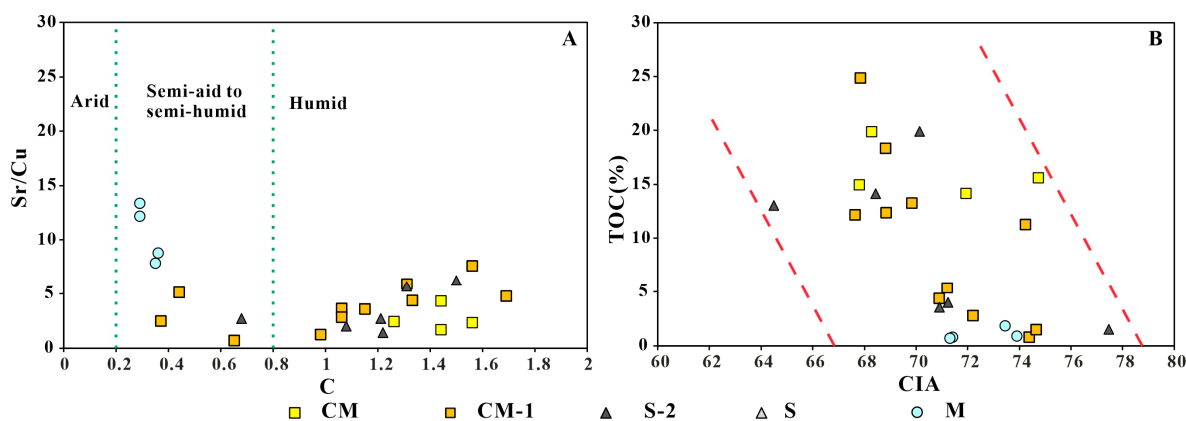


Figure 7. (A) Crossplots of C-value versus Sr/Cu contents. (B) Crossplots of CIA versus TOC contents for paleo-climate of the Chang 7 member in the Ordos Basin.

In the Late Triassic, the world experienced volcanic eruptions and the Carnian Pluvial Episode, during which extreme climate occurred frequently [46]. During the period of lacustrine transgressive system tract and early highstand system tract, the lacustrine basin area reached the maximum, and the lake level peaked. As shown in Figure 7, the comprehensive paleoclimate indicators show that the climate was a mainly semi-humid to humid environment. At this time, the sedimentation rate decreased, and clayey lithofacies were more easily enriched. Frequent volcanic activities led to the increase of CO₂ and other greenhouse gas concentrations, which greatly damaged the terrestrial ecosystem, resulting in enhanced water cycle and surface weathering, and enhanced terrigenous input. In the late Chang 7 Mb. (late highstand system tract), the lake basin gradually shrank, the sedimentary climate gradually changed to a semi-arid environment, and siliceous minerals and carbonate minerals increased. The occurrence frequency of mixed and silty lithofacies increased [20,31,32,46].

5.1.2. Redox Conditions

Relevant studies show that trace elements such as U, V, Cr, Co, and Ni are sensitive to specific redox environments, and their enrichment is greatly controlled by redox conditions of sedimentary environments [47–49]. In other words, they tend to migrate under oxidizing conditions and to precipitate under reductive conditions [30,40–42]. It is easy to preserve U under reductive conditions. U diffuses into sediments in the form of UO₂(CO₃)₃⁴⁻ and is reduced to UO₂, U₃O₇, and U₃O₈, which are enriched in sediments and have high solubility under oxidizing conditions [40]. Th is a relatively inert element that tends to accumulate in clay [31]. Therefore, $\delta U = 2U/(Th/3+U)$ is often used to characterize paleo-redox conditions of sedimentary environments. Specifically, $\delta U < 1$ represents an oxidizing environment, while $\delta U > 1$ represents a reductive environment [40].

V/Cr is used to identify the paleo-redox environment. It is generally considered that V is adsorbed in hydroxide or kaolinite of Fe and Mn in the form of HVO₄²⁻ and H₂VO₄⁴⁻ under oxidizing conditions. When the oxygen content decreases gradually, V(V) is reduced to V(IV) and V(III), which are adsorbed in porphyrin or precipitate in the form of oxide [42]. Similar to V, Cr dissolves in water in an oxidizing environment and precipitates in a reductive environment. However, V/Cr has different values due to denitrification. Generally, V/Cr > 4.25 indicates a highly reductive environment, and V/Cr < 2.00 indicates an oxidizing environment [40,50].

Co and Ni are both sulfur-preferring and dissolve in water in the form of divalent ions. In a highly reductive environment with free H₂S, they do not change their valence, and instead form sulfides and enter into pyrite. Usually, Ni/Co < 5 indicates an oxidation environment, while Ni/Co > 7 represents a reductive environment [50]. Fe/Al is also indicative of redox conditions. In most cases, Fe content is directly proportional to the reducibility, and higher Fe/Al values suggest deep-water reductive environments [15,36].

As shown in the redox index cross-plots (Figure 8A,B), the mixed mudstone facies (M) correspond to an oxidizing environment, while the clay shale facies (CM), silty shale facies (CM-1), and argillaceous siltstone facies (S-2) are mainly deposited in an oxygen-deficient reductive environment. δU in the study area is 0.84–1.95, with an average of 1.62. Figure 8A illustrates that the δU of the mixed mudstone facies (M) is 0.87, and the difference of δU values in other facies is small. Moreover, Ni/Co of the mixed mudstone facies (M) is 2.33; that of the clayey shale facies (CM) is 4.61; that of the silty shale facies (CM-1) is 4.26; that of the argillaceous siltstone facies (S-2) is 5.92. This may be due to the fact that Ni in the deposited organic complex will be re-released into the upper water or pore water in a moderately reductive environment in the absence of H₂S and oxides of Fe and Mn, which results in low Ni/Co [39]. The V/Cr values of the M, CM, CM-1, and S-2 lithofacies are 1.20, 3.74, 3.04, and 3.14, respectively, which indicate that the sedimentary environment of the Chang 7₂₊₃ is mainly a weak oxidation–weak reduction environment; that of the mixed mudstone facies corresponding to the Chang 7₁ is mainly an oxidation environment.

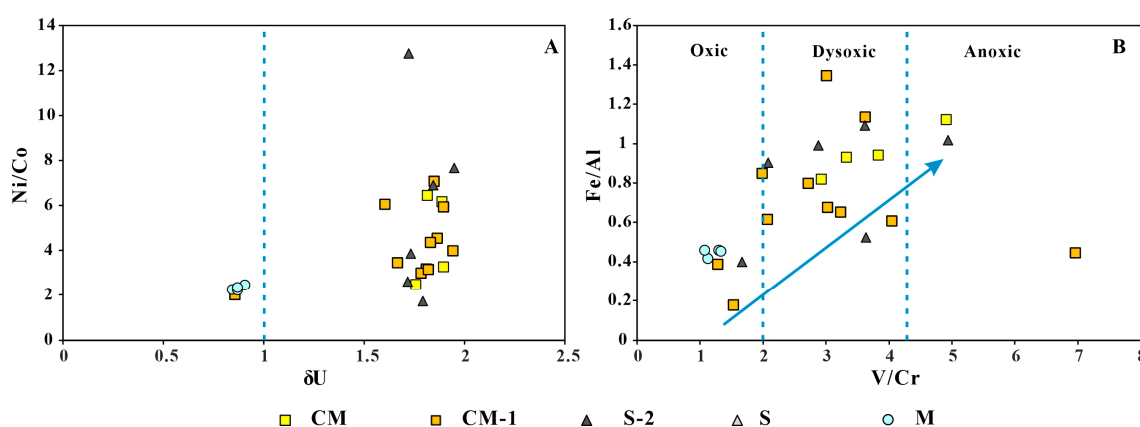


Figure 8. (A) Crossplots of δU versus Ni/Co contents. (B) Crossplots of V/Cr versus Fe/Al contents for redox conditions of the Chang 7 Member in the Ordos Basin.

In summary, the alternative indexes of redox conditions indicate the preservation conditions of fine-grained sediments [39–41]. In the middle and lower part of the Chang 7 Mb., the lake basin reached the maximum flood surface, and the bottom water condition was a dysoxic to anoxic environment. At the same time, the Qinling orogenic belt activity led to the increase of volcanic activity, and the intense marginal volcanic activity intensified the stable subsidence of the basin and the lake basin expansion [19]. Volcanic ash can not only form clay minerals such as montmorillonite and chlorite after entering the water but also cause the death of organisms in the euphotic zone, which aggravates the reduction conditions of the lake basin and is conducive to the preservation of clay minerals. The lithofacies in this period are mainly clay lithofacies [46]. In the late Chang 7 Mb., the lake basin water became shallower, the limit of redox changed from water to sediments, the bottom water environment became an oxic environment, and mixed and silty rock facies appeared frequently.

5.1.3. Paleoproductivity

Some trace elements (such as P and Cu) can be used to characterize the paleoproductivity. P is an important nutrient element for algae growth, and Cu often participates in the formation of organometallic complexes [37,46,51–55]. In order to eliminate the influences of terrigenous detritus, the two elements were divided by Ti to construct the indexes of primary productivity of lake basins. High P/Ti and Cu/Ti indicate higher primary productivity. As shown in Cu/Ti versus TOC (Figure 9A), they are directly proportional to each other, which means that with the increase of primary productivity, the organic matter content in sediments also increases. The Cu/Ti values of the M, CM, CM-1, and S-2 lithofacies are 0.007, 0.048, 0.040, and 0.037, respectively, showing an overall trend of

increasing paleo-productivity. P in sedimentary basins is usually deposited and attached to organic matter. The sensitivity of P to redox conditions is related to the reducibility of iron hydroxide, and its occurrence form depends on the redox conditions of basal water [52]. In the reductive basal water environment, organic P is released via organic matter degradation and diffuses into pore water of overlying strata; moreover, some escape from sediments [53]. In the oxidizing basal water environment, P formed by remineralization is enriched in sediments through adsorption, complexation reactions, and biological isolation of polyphosphate. Such capture mechanisms of P lead to the formation of conditions conducive to the enrichment of authigenic phosphate minerals in the pore water of sediments. Hence, P is mainly enriched in the position with frequent redox exchange (Figure 9B) [54]. The P/Ti values of the M, CM, CM-1, and S-2 lithofacies are 0.18, 0.61, 0.40, and 0.42, respectively, and the average value of the Chang 7 Mb. is 0.40. The overall trend is that the detrital content decreases with the increase of the clay content. In other words, P/Ti declines, and the paleo-productivity decreases in a regression environment (from the Chang 7₃ to Chang 7₁).

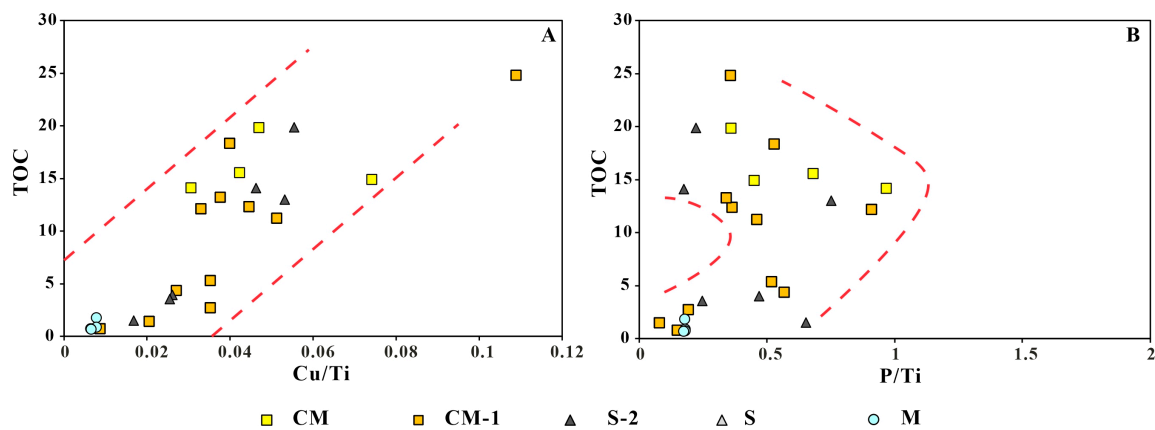


Figure 9. (A) Crossplots of Cu/Ti versus TOC contents. (B) Crossplots of P/Ti versus TOC contents for paleo-productivity of the Chang 7 Member in the Ordos Basin.

Biological cycling is closely related to the oxygen contents of the sedimentary basin. In the Yanchang Fm., biological prosperity contributed to the nutrients (Fe, P, N, Si, Mn) imported by volcanic activities, which promoted the development of algae in the water column. Meanwhile, volcanic ash reacted with gases such as SO₂ and dissolved in the lake basin to trigger microbial sulfuric acid reduction, which slightly reduced the paleoproductivity [52]. However, a strong reducing environment was generated, which facilitated the formation of organic-rich black mud shale (Figure 5B,F). During the Chang 7₁, volcanic activity weakened, the water body became shallower, and primary productivity decreased significantly. Therefore, paleoproductivity had a greater impact on the early Chang 7 Mb. [18–20,25,28,30].

5.1.4. Terrigenous Influx

The terrigenous detrital input affects the deposition rate and biodegradation of organic matter, and subsequently, the composition of lithofacies [56]. Ti and Al are often used to identify debris flow. Ti mainly occurs in clay and heavy minerals in sediments, while Al mainly adheres to clay, feldspar, and aluminosilicate minerals. Therefore, Ti and Al are often used to characterize the terrigenous input of shale [29,37,56]. As suggested by TiO₂ versus TOC (Figure 10A), an inversely proportional relationship exists between these two parameters. With the increase of terrigenous material input (the increase of TiO₂), the organic matter content tends to decline. The TiO₂ values of the M, CM, CM-1, and S-2 lithofacies are 0.63, 0.44, 0.53, and 0.46, respectively, which show that with the increase of sandy content from bottom to top, the frequency of debris flow grows, the TiO₂ content increases, and the organic matter content drops. An effective index of non-aluminosilicate

detrital materials can be developed by dividing the Ti content by the Al content. High $\text{TiO}_2/\text{Al}_2\text{O}_3$ values reflect high terrigenous input and high deposition rates [35]. The $\text{TiO}_2/\text{Al}_2\text{O}_3$ values of the M, CM, CM-1, and S-2 lithofacies are 0.043, 0.039, 0.038, and 0.043, respectively, which implies that in the lithofacies with higher detrital content, the $\text{TiO}_2/\text{Al}_2\text{O}_3$ values are relatively higher, indicating higher terrestrial input (Figure 10B). Furthermore, the inverted value of this ratio (averaging 25.46) is mostly greater than 21. Previous studies claim that the intra-continental orogeny began in Qinling during the Middle Triassic, associated with the depression stage of the lake basin in the study area. At the same time, volcanic and seismic activities occurred frequently, due to the collision between the Qinling and North China blocks, which led to the large-scale eruption of rhyolite. Therefore, the high $\text{Al}_2\text{O}_3/\text{TiO}_2$ may imply that the provenance should originate from the felsic igneous rocks in the southern Ordos [26].

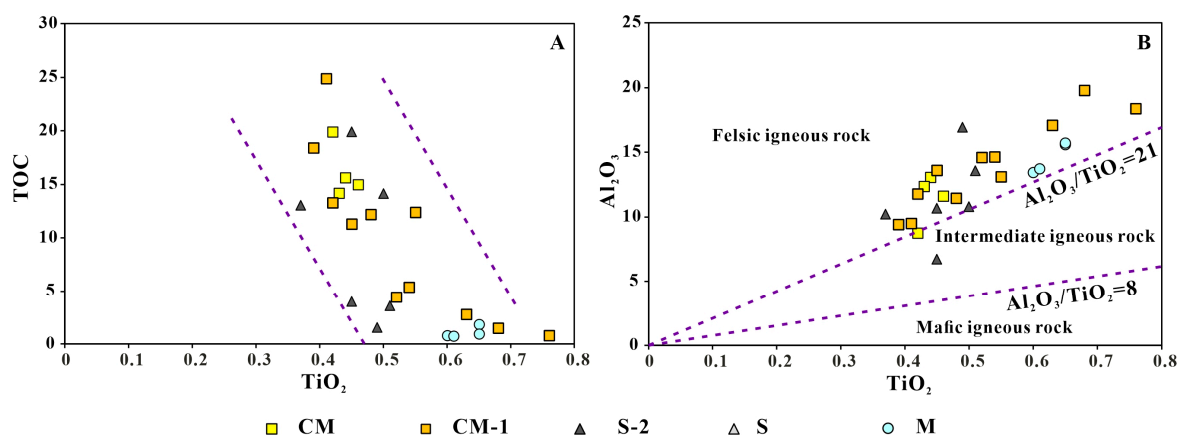


Figure 10. (A) Crossplots of TiO_2 versus TOC contents. (B) Crossplots of TiO_2 versus Al_2O_3 contents for detrital input of the Chang 7 Member in the Ordos Basin.

The input of terrigenous debris can affect the deposition rate and biodegradation of organic matter, thus affecting the composition of lithofacies [56,57]. Sand particles are mainly input into sedimentary basins through rivers, and the increase of silty content indicates that the input of terrigenous debris increases and the occurrence frequency of silty lithofacies increases [34]. Volcanic turbidity events occasionally occur in the middle and lower parts of the Chang 7 Mb. under the overall deep-water background (Figure 2), resulting in increased sand contents, weakened upward tectonic activity, shallower water depth, drier paleoclimate, advancement of terrigenous debris carried by rivers to the center of the lake, strong evaporation, and a water regression environment, which cause undeveloped shale and frequent occurrence of silty and gray minerals. These phenomena demonstrate that terrigenous input has a great influence on the upper part of the Chang 7 Mb. [37].

5.2. Lithofacies Assemblages and Sedimentary Models of Fine-Grained Sediments

During the Late Triassic, influenced by the regional tectonic activities of the Yangtze and North China blocks, the deposition of the Chang 7 Mb. was associated with frequent volcanic activities. Furthermore, the lake basin laterally expanded during the deposition of the Chang 7 Mb., with maximum water depth. The vast area in the southeastern part of the basin (the study area) was in the semi-deep–deep lake environment [18,19]. According to the lithofacies types and genetic mechanisms of the Chang 7 Mb. shale in the study area, two types of lithofacies assemblages are identified. One is developed in a shallow water sedimentary environment of the shore-shallow lake-delta front deposition; the other occurs in a deep–water sedimentary environment of the semi-deep–deep lake deposition.

Lithofacies Assemblage I includes the mixed mudstone and blocky silty mudstone lithofacies and is deposited in the shore-shallow lake or delta front environment at the

margin of the lake basin. It often occurs at the top of the Chang 7₁ and Chang 7₂ (Figure 11). The microscope reveals the underdevelopment of laminations, the dominant blocky structure, and the dotted distribution of organic matter with low TOC (Figure 5C,G,H). This lithofacies assemblage corresponds to an oxidizing sedimentary environment with the cold and arid climate and shallow water depth. The deposition of the Chang 7₁ was less affected by volcanic activities. Due to the cold and arid climate and shallow water depths of the shore-shallow lake-delta front facies, the paleo-productivity of the lake basin was relatively low [17]. The shore-shallow lake-delta front sedimentary facies is subjected to high terrigenous input. A large amount of dissolved oxygen is carried into the water of the lake basin by high terrigenous input, which results in excessive oxygen content. The oxidizing environment of the lake basin leads to massive degradation of organic matter in the lake basin, which consumes a large amount of organic matter stored in shale and leaves the overall low TOC of this lithofacies assemblage. This lithofacies assemblage is also greatly influenced by sandy debris flow on an overall basis; the terrigenous detrital material supply is sufficient, the deposition rate is relatively high so the structure is blocky, the silty and sandy content is high, and the genetic mechanism is mainly turbidity current [18,26].

Lithofacies Assemblage II includes clayey shale facies, laminated silty shale facies, quasi-laminated silty shale facies, and laminated argillaceous siltstone facies. Based on the above paleo-environment analysis, it can be summarized that this lithofacies assemblage is deposited in the deep-water area in the center of the lake basin, and the slope zone of the lake basin located in the deep–shallow water transition zone (Figure 11). During deposition, the climate of this lithofacies assemblage is deposited in a weak oxidation–weak reduction environment with a warm and humid climate, deep water column, and high primary productivity. Microscopically, a ternary structure composed of clay, organic matter, and sandy laminations is observed, and the laminations are linear and wavy (Figure 5E,I). The near-horizontal and slightly wavy laminations indicate that the deep lake had weak hydrodynamics during shale deposition, and the water column of the whole lake basin water body was relatively calm [3]. Fe mainly occurs in shale in the form of pyrite, indicating that shale deposition occurred in an oxygen-deficient environment [36]. Previous studies claim that influenced by the Indosinian movement during the deposition of the Chang 7 Mb., the orogeny in the Qinling area caused frequent volcanic activities and hydrothermal events in the southern part of the basin, which is manifested as the change of some characteristic elements (such as Fe, P, U, and S). Such elements are vital indicators of the blooming of algae, the improvement of primary productivity, the decrease of oxygen content in water (Figure 5B,F), and the formation of the sulfurized water environment during the deposition of the Chang 7 Mb. [17,22,24].

To sum up, the fine-grained sediments of the Chang 7 Mb. have different lithofacies assemblages, due to the change in sedimentary environments. It is considered that under the warm and humid climate conditions beneficial to the growth of aquatic organisms, massive volcanic ashes produced by volcanic activities carry a large number of nutrient elements, such as P and Fe, into the water column of the lake basin, which results in an outburst of algae and other organisms in the lake basin. This provides the material basis for the enrichment of organic matter [18]. Volcanic and hydrothermal activities trigger the blossoming of algae, which produces a lot of organic matter and also consumes oxygen in the lake basin. Therefore, the basal water environment is deficient in oxygen [17,46]. In addition, large-scale multi-stage volcanic activities within a short period of time lead to massive deaths of algae, and hence, organic matter is seasonally and periodically deposited with algal remains, which forms organic matter and clay laminations [3]. Lithofacies Assemblage II is mainly formed in the deep lake-facies environment, which is relatively closed and has high productivity, relatively low terrigenous input, and a low deposition rate. With the gradual shrinkage of the lake basin during the Yanchang stage, the terrigenous input increased, and the water column became more oxidizing. Correspondingly, the lithofacies assemblage gradually changed into Assemblage II, consisting of the mixed mudstone and blocky silty mudstone lithofacies.

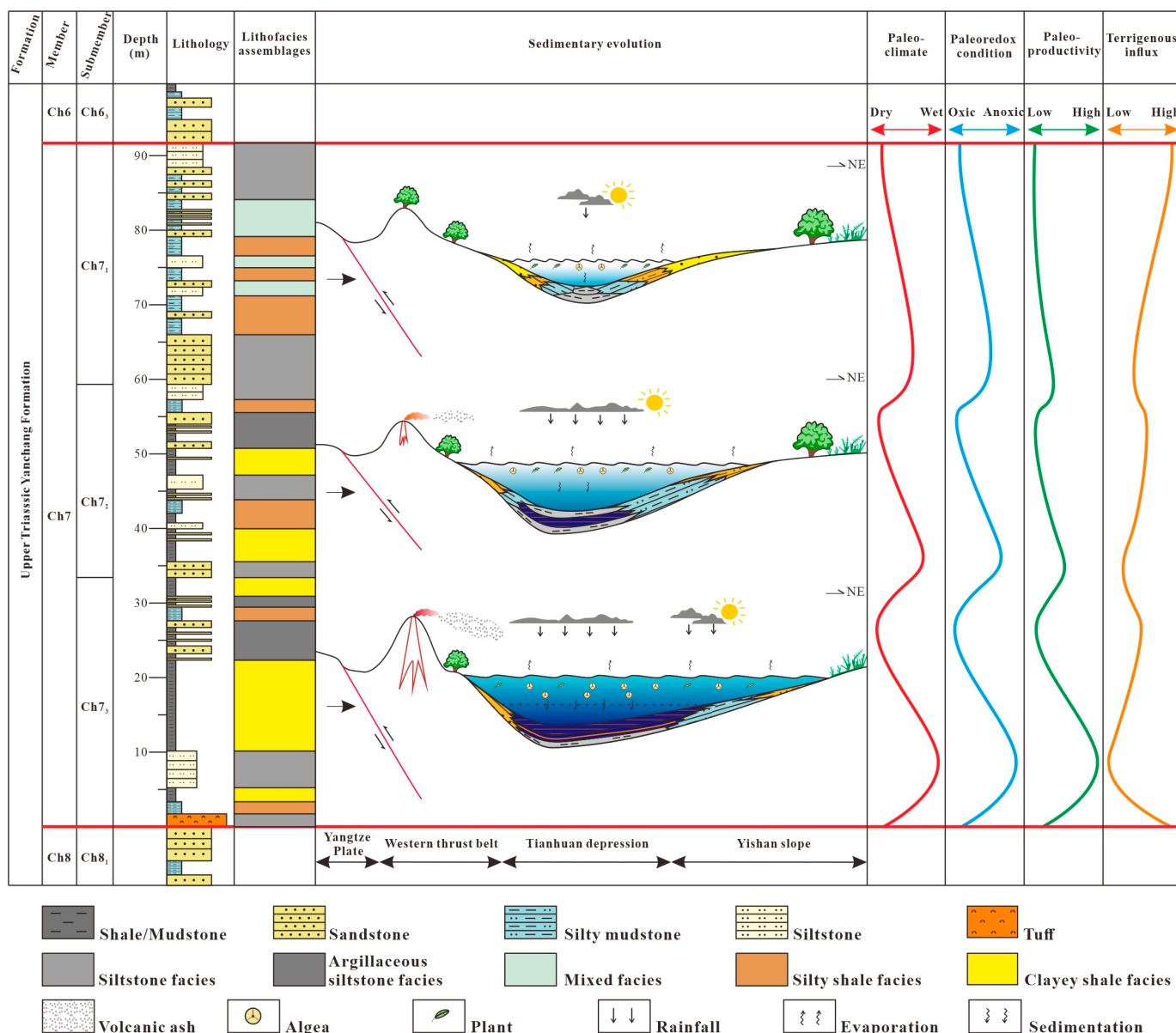


Figure 11. Lithofacies assemblages and sedimentary models of the Chang 7 Member of the Ordos Basin.

6. Conclusions

- (1) In view of the mineral composition content, TOC, structure, texture, and lamination morphology of mudstone/shale, the fine-grained sediments of the Chang 7 Mb. are divided into six lithofacies: quasi-laminated clayey shale, blocky silty mudstone, quasi-laminated silty shale, laminated silty shale, blocky mixed mudstone, and laminated argillaceous siltstone lithofacies.
- (2) Changes in the depositional environment control the petrographic changes in the Ordos Basin. Paleoclimate and terrestrial input have a strong influence on the upper part of the Chang 7 Mb., and paleoproductivity has a greater effect on the lower part of the Chang 7 Mb., while redox conditions play a key role in the preservation of fine-grained sediments. The warm, humid, and anoxic bottom water environment, higher primary productivity, and low terrestrial input are more likely to produce clayey facies, while massive mixed facies and siltstone facies are likely to appear in the upper part of the Chang 7 Mb.
- (3) Two lithofacies assemblages are identified in the Chang 7 Member. The assemblage composed of clayey shale, laminated silty shale, quasi-laminated silty shale, and lami-

nated argillaceous siltstone lithofacies mainly occurs in the deep-water sedimentary environment of the semi-deep–deep lake facies in the lower Chang 7 Member. Moreover, the assemblage of the mixed mudstone and blocky silty mudstone lithofacies is deposited in the shallow-water sedimentary environment or delta facies at the margin of the lake basin.

Author Contributions: Writing—review and editing, Z.C.; writing—original draft preparation, X.L.; validation, H.C.; formal analysis, Z.D.; investigation, Z.Q.; data curation, X.Z.; supervision, Y.H. All authors have read and agreed to the published version of the manuscript.

Funding: This research was funded by the National Natural Science Foundation of China, grant number 41772143.

Data Availability Statement: Not applicable.

Conflicts of Interest: The authors declare no conflict of interest.

References

- Zou, C.; Pan, S.; Horsfield, B.; Yang, Z.; Hao, S.; Liu, E.; Zhang, L. Oil retention and intrasource migration in the organic-rich lacustrine Chang 7 shale of the Upper Triassic Yanchang Formation, Ordos Basin, central China. *AAPG Bull.* **2019**, *103*, 2627–2663. [[CrossRef](#)]
- Liu, M.; Xiong, C. Diagenesis and reservoir quality of deep-lacustrine sandy-debris-flow tight sandstones in Upper Triassic Yanchang Formation, Ordos Basin, China: Implications for reservoir heterogeneity and hydrocarbon accumulation. *J. Pet. Sci. Eng.* **2021**, *202*, 108548. [[CrossRef](#)]
- Li, Z.; Wu, S.; Xia, D.; Zhang, X.; Huang, M. Diagenetic alterations and reservoir heterogeneity within the depositional facies: A case study from distributary-channel belt sandstone of Upper Triassic Yanchang Formation reservoirs (Ordos Basin, China). *Mar. Pet. Geol.* **2017**, *86*, 950–971. [[CrossRef](#)]
- Xue, C.; Wu, J.; Qiu, L.; Zhong, J.; Zhang, S.; Zhang, B.; Wu, X.; Hao, B. Lithofacies classification and its controls on the pore structure distribution in Permian transitional shale in the northeastern Ordos Basin, China. *J. Pet. Sci. Eng.* **2020**, *195*, 107657. [[CrossRef](#)]
- Kane, O.I.; Hu, M.; Cai, Q.; Deng, Q.; Yang, W.; Zuo, M. Sedimentary facies, lithofacies paleogeography, and an evaluation of the Ordovician sequences in the Sichuan Basin, southwest China. *Mar. Pet. Geol.* **2023**, *149*, 106096. [[CrossRef](#)]
- Wang, E.; Guo, T.; Li, M.; Li, C.; Dong, X.; Zhang, N.; Feng, Y. Exploration potential of different lithofacies of deep marine shale gas systems: Insight into organic matter accumulation and pore formation mechanisms. *J. Nat. Gas Sci. Eng.* **2022**, *102*, 104563. [[CrossRef](#)]
- Gao, Y.; Wen, Z.; Xu, Y.; Song, H.; Li, W.; Yu, Y.; Ke, C. Geochemical characteristics of the Chang7 organic-rich fine-grained sedimentary rocks and its relationship with the tight oil in Longdong area, Northwest China. *J. Pet. Explor. Prod. Technol.* **2020**, *10*, 1803–1816. [[CrossRef](#)]
- Mahran, T.; Hassan, A.M. Controls on Late Miocene to Early Quaternary continental sedimentation during the development of the Sohag basin, Nile Valley, Egypt. *J. Afr. Earth Sci.* **2023**, *199*, 104829. [[CrossRef](#)]
- Loucks, R.G.; Ruppel, S.C. Mississippian Barnett Shale: Lithofacies and depositional setting of a Deep-Water Shale-Gas Succession in the Fort Worth Basin, Texas. *AAPG Bull.* **2007**, *91*, 579–601. [[CrossRef](#)]
- Hickey, J.J.; Henk, B. Lithofacies Summary of the Mississippian Barnett Shale, Mitchell 2 T.P. Sims Well, Wise County, Texas. *AAPG Bull.* **2007**, *91*, 437–443. [[CrossRef](#)]
- Fu, J.; Deng, X.; Zhang, X.; Luo, A.; Nan, Q. Relationship between deepwater sandstone and tight oil of the Triassic Yanchang Formation in Ordos Basin. *J. Palaeogeogr.* **2013**, *15*, 624–634.
- Zhou, Z.; Wang, G.; Ran, Y.; Lai, J.; Cui, Y.; Zhao, X. A Logging Identification Method of Tight Oil Reservoir Lithology and Lithofacies: A Case from Chang7 Member of Triassic Yanchang Formation in Heshui Area, Ordos Basin, NW China. *Pet. Explor. Dev.* **2016**, *43*, 61–68. [[CrossRef](#)]
- Xinong, X.; Hongjing, L.; Xiang, X.; Junhua, H.; Jiabin, Y.; Jianzhong, Q.; Tenger, W.; Wu, L. Main controlling factors of organic matter richness in a permian section of guangyuan, northeast sichuan. *J. China Univ. Geosci.* **2008**, *19*, 507–517. [[CrossRef](#)]
- Fathy, D.; Wagreich, M.; Ntaflos, T.; Sami, M. Paleoclimatic variability in the southern Tethys, Egypt: Insights from the mineralogy and geochemistry of Upper Cretaceous lacustrine organic-rich deposits. *Cretac. Res.* **2021**, *126*, 104880. [[CrossRef](#)]
- Ross, D.J.K.; Bustin, R.M. Investigating the use of sedimentary geochemical proxies for paleoenvironment interpretation of the thermally mature organic-rich strata: Examples from the Devonian–Mississippian shales. *West. Can. Sediment. Basin. Chem. Geol.* **2009**, *260*, 1–19.
- Jones, B.; Manning, D.A.C. Comparison of geochemical indices used for the interpretation of palaeoredox conditions in ancient mudstones. *Chem. Geol.* **1994**, *111*, 111–129. [[CrossRef](#)]
- Yuan, W.; Liu, G.; Zhou, X.; Xu, L.; Li, C. Palaeoproductivity and organic matter accumulation during the deposition of the Chang 7 organic-rich shale of the Upper Triassic Yanchang Formation, Ordos Basin, China. *Geol. J.* **2020**, *55*, 3139–3156. [[CrossRef](#)]

18. Yuan, W.; Liu, G.; Stebbins, A.; Xu, L.; Niu, X.; Luo, W.; Li, C. Reconstruction of redox conditions during deposition of organic-rich shales of the Upper Triassic Yanchang Formation, Ordos Basin, China. *Palaeogeogr. Palaeoclimatol. Palaeoecol.* **2017**, *486*, 158–170. [[CrossRef](#)]
19. Yuan, W.; Chen, R.; Liu, G.; Shang, F.; Xu, L.; Niu, X. Linking the Qinling Orogeny with the Chang 7 shale (Triassic Yanchang Formation) deposition: Evidence from major, trace, and rare earth element geochemistry. *Geol. J.* **2019**, *54*, 133–142. [[CrossRef](#)]
20. Zhao, J.; Liu, C.; Huang, L.; Zhang, D.; Wang, D.; Wang, D. Paleogeography reconstruction of a multi-stage modified intra-cratonic basin—A case study from the Jurassic Ordos Basin, Western North China Craton. *J. Asian Earth Sci.* **2020**, *190*, 104191. [[CrossRef](#)]
21. Ruan, Z.; Luo, Z.; Yu, B.; Lu, Y.; Xie, H.; Yang, Z. Middle-Late Triassic basin prototype and tectonic paleographic response in the Ordos Basin. *Earth Sci. Front.* **2021**, *28*, 12–32.
22. Yang, Y.T.; Li, W.; Ma, L. Tectonic and stratigraphic controls of hydrocarbon systems in the Ordos basin: A multicycle cratonic basin in central China. *AAPG Bull.* **2005**, *89*, 255–269. [[CrossRef](#)]
23. Wang, J.; Liu, C.; Guo, Z.; Zhang, D. Sedimentary response of regional tectonic transformation in Late Triassic Yanchang period at the central and southern Ordos Basin central. *Earth Sci. Front.* **2015**, *22*, 194–204.
24. Qiu, X.; Liu, C.; Mao, G.; Wu, B. Petrological-Geochemical Characteristics of Volcanic Ash Sediments in Yanchang Formation in Ordos Basin. *Earth Sci.* **2011**, *36*, 139–150.
25. Yang, H.; Niu, X.; Xu, L.; Feng, S.; You, Y.; Liang, X.; Wang, F.; Zhang, D. Exploration potential of shale oil in Chang7 Member, Upper Triassic Yanchang Formation, Ordos Basin, NW China. *Pet. Explor. Dev.* **2016**, *43*, 511–520. [[CrossRef](#)]
26. Zhang, K.; Liu, R.; Liu, Z. Sedimentary sequence evolution and organic matter accumulation characteristics of the Chang 8–Chang 7 members in the Upper Triassic Yanchang Formation, southwest Ordos Basin, central China. *J. Pet. Sci. Eng.* **2021**, *196*, 107751. [[CrossRef](#)]
27. Pan, S.; Liao, Y.; Jiang, B.; Wan, Z.; Wang, F. Genesis analysis of black rock series: A case study of Chang 7₃ member in tongchuan area. *Acta Sedimentol. Sin.* **2019**, *37*, 1117–1128.
28. Calvert, S.E.; Pedersen, T.F. Chapter fourteen elemental proxies for palaeoclimatic and palaeoceanographic variability in marine sediments: Interpretation and application. *Dev. Mar. Geol.* **2007**, *1*, 567–644.
29. Tribouillard, N.; Algeo, T.J.; Lyons, T.; Riboulleau, A. Trace metals as paleoredox and paleoproductivity proxies: An update. *Chem. Geol.* **2006**, *232*, 12–32. [[CrossRef](#)]
30. Taylor, S.R.; McLennan, S.M. *The Continental Crust: Its Composition and Evolution*; Blackwell Scientific Publications: Oxford, UK, 1985.
31. Fan, M.; Bu, J.; Zhao, X.; Kang, B.; Li, W.; Zhang, W. Geochemical characteristics and environmental implications of trace elements of Yanchang Formation in southeastern Ordos Basin. *J. Northwest Univ.* **2019**, *49*, 633–642.
32. Moradi, A.V.; Sari, A.; Akkaya, P. Geochemistry of the Miocene oil shale (Hançili Formation) in the Çankırı-Çorum Basin, Central Turkey: Implications for Paleoclimate conditions, source–area weathering, provenance and tectonic setting. *Sediment. Geol.* **2016**, *341*, 289–303. [[CrossRef](#)]
33. Nesbitt, H.W.; Young, G.M. Early Proterozoic climates and plate motions inferred from major element chemistry of lutites. *Nature* **1982**, *299*, 715–717. [[CrossRef](#)]
34. Diaz, H.G.; Fuentes, C.C.; Calvin, C.; Yang, Y.; MacPhail, K.; Lewis, R. Evaluating the impact of mineralogy on reservoir quality and completion quality of organic shale plays. In Proceedings of the AAPG Rocky Mountain Section Meeting, Salt Lake City, UT, USA, 22–24 September 2013.
35. Zou, C.; Zhao, Z.; Yang, H.; Fu, J.; Zhu, R.; Yuan, X.; Wang, L. Genetic mechanism and distribution of sandy debris flows in terrestrial lacustrine basin. *Acta Sedimentol. Sin.* **2009**, *27*, 1065–1075.
36. Feng, F. *Enrichment Mechanism of Organic Matter and Geochemical Characteristics of Fe-S-C in Wufeng Formation-Longmaxi Formation in Northeast Chongqing*; China University of Mining and Technology: Beijing, China, 2019.
37. Ma, Y.; Lu, Y.; Liu, X.; Zhai, G.; Wang, Y.; Zhang, C. Depositional environment and organic matter enrichment of the lower Cambrian Niutitang shale in western Hubei Province, South China. *Mar. Pet. Geol.* **2019**, *109*, 381–393. [[CrossRef](#)]
38. Yuan, W.; Liu, G.; Bulseco, A.; Xu, L.; Zhou, X. Controls on U enrichment in organic-rich shales from the Triassic Yanchang Formation, Ordos Basin, Northern China. *J. Asian Earth Sci.* **2021**, *212*, 104735. [[CrossRef](#)]
39. Rimmer, S.M. Geochemical paleoredox indicators in Devonian–Mississippian black shales, Central Appalachian Basin (USA). *Chem. Geol.* **2004**, *206*, 373–391. [[CrossRef](#)]
40. Emerson, S.R.; Huested, S.S. Ocean anoxia and the concentrations of molybdenum and vanadium in seawater. *Mar. Chem.* **1991**, *34*, 177–196. [[CrossRef](#)]
41. Lyons, T.W.; Werne, J.P.; Hollander, D.J.; Murray, R. Contrasting sulfur geochemistry and Fe/Al and Mo/Al ratios across the last oxic-to-anoxic transition in the Cariaco Basin, Venezuela. *Chem. Geol.* **2003**, *195*, 131–157. [[CrossRef](#)]
42. Zheng, R.; Liu, M. Paleosalinity study of the Chang 6 oil formation in the Ordos Basin. *Oil Gas Geol.* **1999**, *1*, 22–27.
43. Peng, X.; Wang, L.; Jiang, L. Geochemical Characteristics of the Lucaogou Formation Oil Shale in the Southeastern Margin of the Junggar Basin and Its Environmental Implications. *Bull. Mineral. Petrol. Geochem.* **2012**, *31*, 121–127.
44. Fathy, D.; Abart, R.; Wagreich, M.; Gier, S.; Ahmed, M.S.; Sami, M. Late campanian climatic-continental weathering assessment and its influence on source rocks deposition in southern Tethys, Egypt. *Minerals* **2023**, *13*, 160. [[CrossRef](#)]
45. Qiu, X.; Liu, C.; Mao, G.; Deng, Y.; Wang, F.; Wang, J. Major, trace and platinum-group element geochemistry of the Upper Triassic nonmarine hot shales in the Ordos basin, Central China. *Appl. Geochem.* **2015**, *53*, 42–52. [[CrossRef](#)]

46. Li, Q.; Wu, S.; Xia, D.; You, X.; Zhang, H.; Lu, H. Major and trace element geochemistry of the lacustrine organic-rich shales from the Upper Triassic Chang 7 Member in the southwestern Ordos Basin, China: Implications for paleoenvironment and organic matter accumulation. *Mar. Pet. Geol.* **2020**, *111*, 852–867. [[CrossRef](#)]
47. Hatch, J.R.; Leventhal, J.S. Relationship between inferred redox potential of the depositional environment and geochemistry of the upper pennsylvanian (missourian) stark shale member of the dennis limestone, wabaunsee country, kansas, usa. *Chem. Geol.* **1992**, *99*, 65–82. [[CrossRef](#)]
48. Algeo, T.J.; Maynard, J.B. Trace-element behavior and redox facies in core shales of Upper Pennsylvanian Kansas-type cyclothems. *Chem. Geol.* **2004**, *206*, 289–318. [[CrossRef](#)]
49. Fathy, D.; Wagreich, M.; Sami, M. Geochemical evidence for photic zone euxinia during greenhouse climate in the Tethys Sea, Egypt. In *Proceedings of the Advances in Geophysics, Tectonics and Petroleum Geosciences*; Meghraoui, M., Sundararajan, N., Banerjee, S., Hinzen, K.-G., Eshagh, M., Roure, F., Chaminé, H.I., Maouche, S., Michard, A., Eds.; Springer International Publishing: Cham, Switzerland, 2022; pp. 373–374.
50. Lin, Z.; Chen, D.; Liu, Q. Geochemical indices for redox conditions of marine sediments. *Bull. Mineral. Petrol. Geochem.* **2008**, *27*, 72–80.
51. Piper, D.Z. Seawater as the source of minor elements in black shales, phosphorites and other sedimentary rocks. *Chem. Geol.* **1994**, *114*, 95–114. [[CrossRef](#)]
52. Raiswell, R.; Buckley, F.; Berner, R.A.; Anderson, T.F. Degree of pyritization of iron as a paleoenvironmental indicator of bottom-water oxygenation. *J. Sediment. Petrol.* **1988**, *58*, 812–819.
53. Algeo, T.J.; Ingall, E. Sedimentary Corg:P ratios, paleocean ventilation, and Phanerozoic atmospheric pO₂. *Palaeogeogr. Palaeoclimatol. Palaeoecol.* **2007**, *256*, 130–155. [[CrossRef](#)]
54. Ingall, E. Sediment carbon, nitrogen and phosphorus cycling in an anoxic fjord, Effingham Inlet, British Columbia. *Am. J. Sci.* **2005**, *305*, 240–258. [[CrossRef](#)]
55. Gabriel, M.F. The Global Phosphorus Cycle. *Rev. Mineral. Geochem.* **2002**, *48*, 391–425.
56. Canfield, D.E. Factors influencing organic carbon preservation in marine sediments. *Chem. Geol.* **1994**, *114*, 315–329. [[CrossRef](#)] [[PubMed](#)]
57. Zhang, J.; Lu, Y.; Krijgsman, W.; Liu, J.; Li, X.; Du, X.; Wang, C.; Liu, X.; Feng, L.; Wei, W.; et al. Source to sink transport in the Oligocene Huagang Formation of the Xihu Depression, East China Sea Shelf Basin. *Mar. Pet. Geol.* **2018**, *98*, 733–745. [[CrossRef](#)]

Disclaimer/Publisher's Note: The statements, opinions and data contained in all publications are solely those of the individual author(s) and contributor(s) and not of MDPI and/or the editor(s). MDPI and/or the editor(s) disclaim responsibility for any injury to people or property resulting from any ideas, methods, instructions or products referred to in the content.